



Research Article

The Effect of the Nano-Drug Carbomicin Inhibiting the Relapse of Stomach Cancer after Radiofrequency Ablation

Yueting Li¹, Baoquan Zhao^{2✉}, Yunzhu Pu², Weitong Pan³, Xiaoman Li², Yuxia Wang²
Yongan Wang², Lan Sun², Chunqian Huang², Qian Li², Yingge Zhang^{2✉}

¹Department of Surgery, Beijing Hospital of Integrated Traditional and Western Medicine, Beijing 100039, China.

²State Key Laboratory of Toxicology and Medical Countermeasures, Institute of Toxicology and Pharmacology, Academy of Military Medical Sciences, Beijing 100850, China.

³Institute of Materia Medica, Chinese Academy of Medical Sciences and Peking Union Medical College, Beijing 100050, China.

✉ Corresponding authors. E-mail: baoquanzhao@126.com; zhangygm@126.com

Received: Dec. 20, 2017; **Accepted:** Dec. 24, 2017; **Published:** Dec. 30, 2017.

Citation: Yueting Li, Baoquan Zhao, Yunzhu Pu, Weitong Pan, Xiaoman Li, Yuxia Wang, Yongan Wang, Lan Sun, Chunqian Huang, Qian Li, and Yingge Zhang, The Effect of the Nano-Drug Carbomicin Inhibiting the Relapse of Stomach Cancer after Radiofrequency Ablation. *Nano Biomed. Eng.*, 2017, 9(4): 344-354.

DOI: 10.5101/nbe.v9i4.p344-354.

Abstract

Radiofrequency ablation (RFA) is a promising tumor treatment in clinics, but its use is limited given the high post-RFA recurrence rate. To overcome tumor relapse, RFA needs to be used in combination with a long-lasting treatment. Obviously, the focal injection of antitumor drugs is capable of increasing the effective treatment period. Nano drug delivery systems (NDDS), which allow for a controlled and slow release of drugs, provide a promising strategy to overcome post-RFA tumor recurrence. Our results showed a clear transit area, between the non-ablation tumor area and the ablation necrotic area, indicative of apparent histopathological partition. Focal injection of the NDDS in combination with focally-injected carbomicin (CBMC) is an effective assistant treatment for RFA, as it increases efficiency and inhibits tumor relapse. Focally injected CBMC is a novel strategy which overcomes the disadvantages of RFA and may even cure it.

Keywords: Radiofrequency ablation; Tumor treatment; Active carbon nanoparticles; Nano drug delivery system; Tumor recurrence

Introduction

Cancer is a worldwide disease. According to a statistical analysis conducted by the American Cancer Society, cancer is estimated to result in 580,350 patient deaths in 2013. Globally, approximately 1,600 people are diagnosed with cancer each day, which is an estimated 1,660,290 new cancer cases per year [1]. Despite the efforts to treat cancers, the 5-year survival rate of 68% for all cancers diagnosed between

2002 and 2008 is still low. For this reason, we need to continue our efforts to find more effective cancer treatments and to reduce mortality rates in clinical practice. Radiofrequency ablation (RFA) is a local thermal damage-based minimally invasive treatment and has, since its first use in 1993 by Rossi et al. [2], slowly gained traction in the research community. RFA treatment is characteristic of only slight trauma, light postoperative pain, quick recovery, strong repeatability, wide indications etc. Furthermore, the RFA treatment

effect is comparable to that obtained with surgical resection. At first, RFA was mainly used for the treatment of primary liver cancer or liver metastasis caused by other tumors [3]. Recently, along with the clinical application, RFA has been used to treat various types of cancers, including kidney cancer, lung cancer, breast cancer, and colorectal cancer [4-7]. However, clinical practice has highlighted some shortcomings of RFA, one of which is its high postoperative recurrence rate. How to subdue these relapses has become the main concern for practitioners.

The principle of RFA treatment is to produce a quick-returned, alternating RF electric field in the local tumor. This stimulates ions to quickly move back and forth inside the RF electric field, thereby generating heat through friction and producing a local high temperature. The latter, in turn, will induce coagulative necrosis of the tumor tissue [8]. Based on the temperature distribution and histopathological changes in the tissue during the process of radio frequency, there are four treatment areas: the application area, the central area, the transition area, and the reference area [9]. The application area and the central area feature the highest temperatures, ranging between 60-300 °C. Because these temperatures can instantly kill tumor cells, this is also referred to as the direct damage effect. The temperature in the transition area reaches 42-60 °C. This inactivates partial enzymes and damages mitochondria and other organelles. Cancer cells in this area are subject to indirect damage effects and exert apoptosis. The reference area is not significantly affected by the temperature (< 42 °C) and would not induce cell death [10]. The scope of direct damage by RFA is, therefore, determined by the tissue volume obliterated by the high temperature. The surviving cells, within the transition zone, and the intact tumor cells, in the reference zone and beyond, constitute the RFA postoperative residual tumor and are believed to be the main cause of tumor recurrence. Based on the principles of post-RFA recurrence, we propose two strategies to overcome post-RFA recurrence. One could either simply expand the scope of ablation, thereby reducing the number of residual tumor cells, or one use other methods in conjunction to inhibit the proliferation of the residual tumor cells.

Local injection of therapeutic agents is widely used in cancer treatment as an assistant chemotherapy to clear the residual cancer cells [11-13] and reduce the prevalence of post-operation relapses [14-18]. One can argue that the principles of such local injections are

also applicable to RFA treatment. If anti-tumor drugs were injected in the RFA focuses, a synergistic effect of the drugs and RFA could be obtained. Recently, it has been noted that the residence time of drugs in the therapeutic site is also an important factor to consider when improving the drug effect [14, 18, 19]. So, in order to increase the effectiveness of the therapeutic agent, one has to establish its effective concentration as well as its residence time. However, thus far, focally injected molecular drugs have not usually maintained an effective concentration for a sufficient amount of time as they are easily absorbed into the blood and lymph capillaries surrounding the RFA focus. Controlled-release nano drugs [28-30] are larger [20-24] than the vascular endothelial pores and gaps of the blood and lymph capillaries [25-27]. Nano drugs are also characterized by an outstanding residence time in the target tissues [31, 32]. They are therefore promising candidates for assistant chemotherapy of RFA. This research studied the treatment effects of RFA in combination with focally-injected carbomicin (CBMC), a nano drug with activated carbon nanoparticles (ACNP) as carriers for mitomycin C (MMC) [33]. CBMC has previously been used successfully to treat stomach cancer due to an increased residence time in peritoneal and lymph tissues following an intraperitoneal injection [34].

Experimental

Instruments and materials

ACNP with a mean diameter of 250 nm were made from medical carbon [35] in our laboratory. Human BGC-823 gastric cancer cells were obtained from the Beijing Institute of Pharmacology and Toxicology, Academy of Military Medical Sciences. Male nude mice (15-20 g) were supplied by the Vital River Company, China. MMC (Kyowa Hakko Kogyo Co., Ltd.), high glucose Dulbecco's modified Eagle medium (Gibico, United States), fetal bovine serum (Hangzhou Sijiqing Biological Engineering Co., Ltd., China), and all other chemical agents were of analytically purity. The MODEL1500XRF instrument was a product of IHTA, United States.

Preparation and characterization of ACNP and CBMC

ACNP were prepared as described elsewhere by ball milling, suspension-precipitation, and freeze drying [36]. To make CBMC, the prepared ACNP was mixed with MMC in a 5:1 mass ratio in triple distilled water.

The mixture was placed in an ultrasound field for 20 min, allowing the MMC to be fully absorbed into the mesopores of the ACNP. Afterwards, high-speed centrifugation was used to remove the unabsorbed MMC. The precipitate was freeze-dried to obtain CBMC powder and was stored at 4 °C for future use. The supernatant of unabsorbed MMC was analyzed by HPLC to estimate the uptake of MMC by the ACNP. CBMC drug loading was calculated using the formula $Q = (C_0 - C_s)V/M$, where Q is the drug loading; C_0 and C_s are, respectively, the MMC concentration at the start and end of adsorption (mg/mL); V is the volume of the adsorption system (mL); and M is the mass of ACNP (mg). By manipulating the ACNP to MMC ratio, CBMC with a drug loading of 0.2 was obtained. Transmission electron microscope and atomic force microscope (AFM) were used to observe the particle size and shape of the prepared CBMC [41]. A laser granularity scatterometer was used to measure the hydrodynamic diameter of CBMC. In order to determine drug release kinetics, 200 mg CBMC was added to 100 mL of tissue fluid obtained by collecting the supernatant of the high-speed centrifuged (20000 rpm, 10 min) tumor tissue homogenate. The MMC concentration in the tissue fluid was determined at different time points after adding CBMC, and the residual drug loading at time $t(Q_t)$ was calculated as $Q_t = (MQ_0 - VC_t)/M$, where M is the mass of ACNP; Q_0 is the drug-loading at the start of the release; V is the volume of tissue fluid; and C_t is the MMC concentration at time t . A drug loading-time (Q - T) curve was obtained by plotting the drug loading against time. The drug release was simulated with first order kinetics. The release constant (k) was calculated as $k = 2.303 (\log Q_0 - \log Q_t)/t$, and the half-releasing time ($t_{1/2}$) was calculated as $t_{1/2} = 0.693/k$.

Establishing cancer models

Human stomach cancer BGC-823 cells were cultured in high glucose Dulbecco's modified Eagle medium containing 10% fetal bovine serum in an atmosphere of 5% CO₂ at 37 °C. The culture medium was changed every two days. At the logarithmic growth phase, the cells were digested with 0.15% trypsin. The digested cells were collected and re-suspended in culture medium and the cell concentration was adjusted to 2×10^6 /mL. Of this cell suspension, 0.2 mL (4×10^5 cells) was injected beneath the skin, in the armpit of the nude mice. The tumor formation was monitored every day and tumor-bearing mice were used in our experiments. A vernier caliper was used to measure

the length (a) and width (b) of the tumor body, and the tumor volume (TV) was calculated as $V = a \times b^2/2$, indicating the tumor size. The actual size of the tumor reported equated to the total size minus the scab size.

Experimental groups

Thirty tumor-bearing nude mice were randomly divided into five groups: A blank control group, an RFA only group, an RFA+ACNP group, an RFA+MMC group and an RFA+CBMC group. In the RFA only group, RFA was performed without drug treatment. In the RFA+ACNP group, 5 mg/kg ACNP (corresponding to the quantity of ACNP contained in CBMC) was injected into the RFA focuses immediately after RFA treatment. In the RFA+MMC group, 1 mg/kg MMC (corresponding to the quantity of MMC contained in CBMC) was injected into the RFA focuses immediately after RFA treatment. In case of RFA+CBMC, 6 mg/kg CBMC, containing 5 mg ACNP and 1 mg MMC, was injected into the RFA focuses immediately after RFA treatment. In addition, the blank control group did not receive any treatment.

In vivo RFA of tumors

RFA treatment was applied when the minimum diameter of the subcutaneous transplantation tumor reached 1.5 cm. The mice were anesthetized by intraperitoneal injection of 0.004 mL/g of 10% chloral hydrate. After anesthesia, the mice were fixed on the electrode plate and care was taken that there was no insulation material between the electrode plate, the nude mice, and the RF needle. Alcohol cotton balls were used to disinfect the tumor position and the RF needle. The RF frequency was set at 500 kHz and the power at 5 W. The upper limit of the temperature was 70 °C. After the RF conditions were set, the RF electrode was inserted along the vertical axis into the tumor center and connected to the power supply. When the RF temperature reached 60 °C, the timing for ablation commenced. The mice received 2 min of ablation therapy. The RFA mice were put back into the cage and kept warm until they were awake.

Drug treatment of tumors in combination with RFA

MMC was dissolved in normal saline at a final concentration of 1 mg/mL. ACNP and CBMC were also suspended in normal saline at respective concentrations of 5 mg/mL and 6 mg/mL. As a result, the liquid volume injected into the RFA focuses was the same for all experimental groups (1 mL CBMC

contained 5 mg ACNP and 1 mg MMC). Before injection, the ACNP and CBMC suspension was vortexed. As mentioned above, the various drugs were focally injected immediately after RFA treatment. This injection was carried out with a microsyringe along the route of the RF electrode and penetrated to the same depth. The drugs were injected in bolus in the center of the RFA focuses.

Monitoring of tumor growth after RFA

Following RFA of the nude mice, tumor length (a) and width (b), together with the length (a1) and width (b1) of the ablation zone, were measured on days 0, 3, 9 and 15. TV (tumor volume) and the ablation volume (AV) were calculated as $V \text{ (mL)} = a \times b^2/2 \text{ (cm}^3\text{)}$. Tumor growth curves (TGC) were drawn by plotting TV against time. Ablation volume ratios (AVR) were calculated as $AVR(\%) = AV/TV \text{ before RFA} \times 100\%$, and the anti-tumor rate (%) = $(1-TV \text{ of the treatment group}/TV \text{ of the control group}) \times 100\%$.

Histopathological observation of post-RFA tumor

On days 0, 3, 9 and 15 after RFA, the tissues from the edge of the RFA focuses were sampled and fixed in 4% paraformaldehyde for 24 hours. Following dehydration, they were embedded, sectioned, dewaxed, dyed and section sealed. Next, hematoxylin and eosin (HE) stain was used to observe histopathological changes in the samples under a light microscope. Pictures were collected with an Olympus digital section workstation.

Immunohistochemical detection of tumor cell proliferation and apoptosis

The paraffin sections of the biopsy samples were dewaxed, hydrated and rinsed in phosphate buffered saline using a routine method. Rabbit anti-caspase 3 and rat anti-proliferating cell nuclear antigen (anti-PCNA) antibody dilutions were added and incubated overnight at 4 °C. On the next day, the sections were rinsed in phosphate buffered saline before adding goat anti-rabbit rhodamine and sheep anti-rabbit FITC for another hour at 37 °C. The sections were again rinsed in phosphate buffered saline, dyed with DAPI, and sealed with fluorescence quenching tablets. The slides were analyzed with a fluorescent microscope and the pictures were collected with an Olympus digital section workstation.

Statistical method

The data were processed with SPSS19.0 statistical

software and the results were expressed as the means \pm standard deviation. Based on one-way analysis of variance, $p < 0.05$ was considered to be of statistical significance.

Results and Discussion

Characterization of CBMC

Observations of the ACNP preparations with an AFM showed spherical particles with a mean particle size of 240 nm and an aspecific surface area of 1400 m²/g (Fig. 1(a)). The mean hydrodynamic diameter of ACNP is 250 nm (Fig. 1(b)), which is slightly larger than estimated by AFM. Further, ACNP had densely distributed micropores of 1-5 nm (Fig. 1(c)), which were visible on the particle surface with a transmission electron microscope (Fig. 1(d)). These micropores formed the structural foundations for the adsorption and release of MMC. The drug loading of CBMC was 0.2. Drug release C-t curves of CBMC are shown in Fig. 1(e)-(g). The data showed that for 2000 mg CBMC in 100 mL of tissue fluid and a surrounding blood flow of 4 $\mu\text{L/s}$, the drug release rate constant was 4.06×10^{-8} and the half-life of the drug release was 1.71×10^7 s (\pm 198 days). At different doses, CBMC drug-releasing curves were identical in shape, with the same drug release constant and half-life, even though the total MMC in the system was significantly different (Fig. 1(e)). In spite of the difference in doses, there was only a slight difference in the concentration of free MMC (Fig. 1(f)), reflecting the ability of CBMC to control the MMC concentration. Compared to free MMC, the residual drug loading of CBMC was strongly influenced by the doses (Fig. 1(g)), suggesting that CBMC maintained the MMC concentration by releasing more MMC into the tissue fluid when the MMC concentration decreased. Although CBMC could control the release of MMC, lower doses had a short effective concentration keeping time (ECKT, Fig. 1(g)). Taken together, the dose of CBMC was shown to significantly influence MMC ECKT but not the concentration of MMC that is released. This mechanism clearly requires further studies.

Stomach cancer models and the growth of tumors

Stomach cancer models were successfully established by implanting human stomach cancer cells beneath the armpit skin of nude mice. By day seven, the tumors were clearly visible in the cell injection site. By day 14 after implanting, the tumor size had

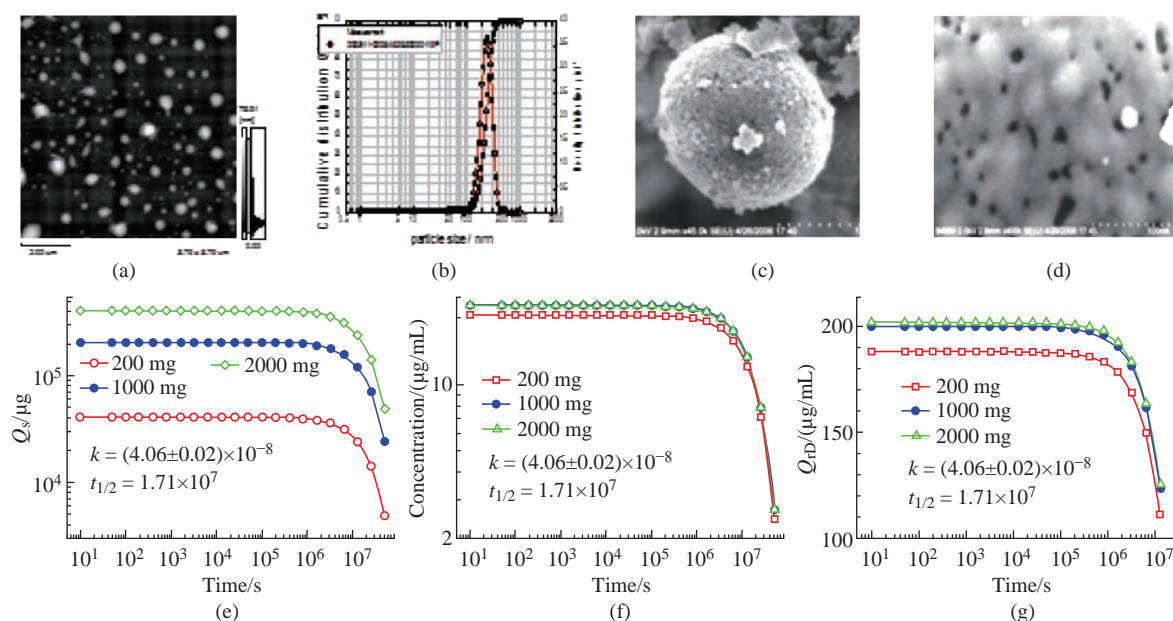


Fig. 1 Characterization of CBMC form and drug release kinetics. (a) CBMC atomic force microscope imaging. (b) CBMC hydrodynamic diameter distribution. (c) CBMC particles under the scanning electron microscope. (d) CBMC surface microporosity. (e) MMC dose-time (Q_s -t) curve in solution. (f) MMC concentration-time (C-t) curve in solution. (g) CBMC drug loading-time (Q_{rd} -t) curve.

increased to 1.5 cm in minimal diameter, which is when the mice models were used for our study.

The effects of the drug treatment on the RFA damage ratio

RFA had excellent temporary therapeutic effects as shown in Fig. 2. Within one day after RFA, the tumor completely disappeared and a scab had formed over the RFA focuses (Fig. 2). The tumor ablation volumes of nude mice following the treatment are shown in Fig. 2. One day after RFA, the damage volume ratio was 22.18% in the RFA only group, 24.92% in the RFA+ACNP group, 45.36% in the RFA+MMC group, and 78.79% in the RFA+CBMC group. As expected,

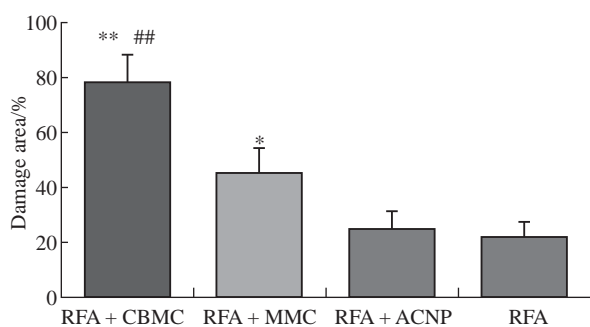


Fig. 2 The tumor ablation volume of nude mice for each treatment group. Note: **, $p < 0.01$, comparison of the RFA only and the RFA + ACNP group; *, $p < 0.05$, comparison of the RFA only and the RFA + ACNP group; ##, $p < 0.01$, comparison of the RFA only and the RFA + MMC group.

the tumor damage volume ratios for the RFA + CBMC and RFA+MMC groups were significantly greater than for the RFA only and RFA+ACNP groups ($p < 0.05$). In addition, the tumor damage volume ratio for the RFA+CBMC group was significantly higher than for the RFA+MMC group ($p < 0.01$). These results indicated that the post-RFA focal injection of drugs synergistically increased the therapeutic effects.

The effects of the drug treatment on post-RFA tumor recurrence

Because the model mice were kept alive following the treatment, tumors relapsed and gradually grew from the edge of the post-RFA scab. Tumor recurrence was assessed at 15 days posttreatment. In RFA only treated mice, multiple small residual tumors fused to form a new large irregular tumor surrounding the scab (Fig. 3), indicating the relapse of the tumor after RFA. Similar sizes of post-RFA recurring tumors were observed in the RFA+ACNP group, indicating that the ACNP treatment in combination with RFA did not significantly impact the tumor relapse. In the RFA+MMC group, however, the recurrent tumors were smaller than in the RFA only group ($p < 0.05$; Fig. 4), indicating that MMC in combination with RFA had some inhibitive effect on tumor recurrence. In the RFA+CBMC group, the sizes of post-RFA recurrent tumors were even smaller than those in the RFA+MMC group ($p < 0.05$; Fig. 4), implying that CBMC was a

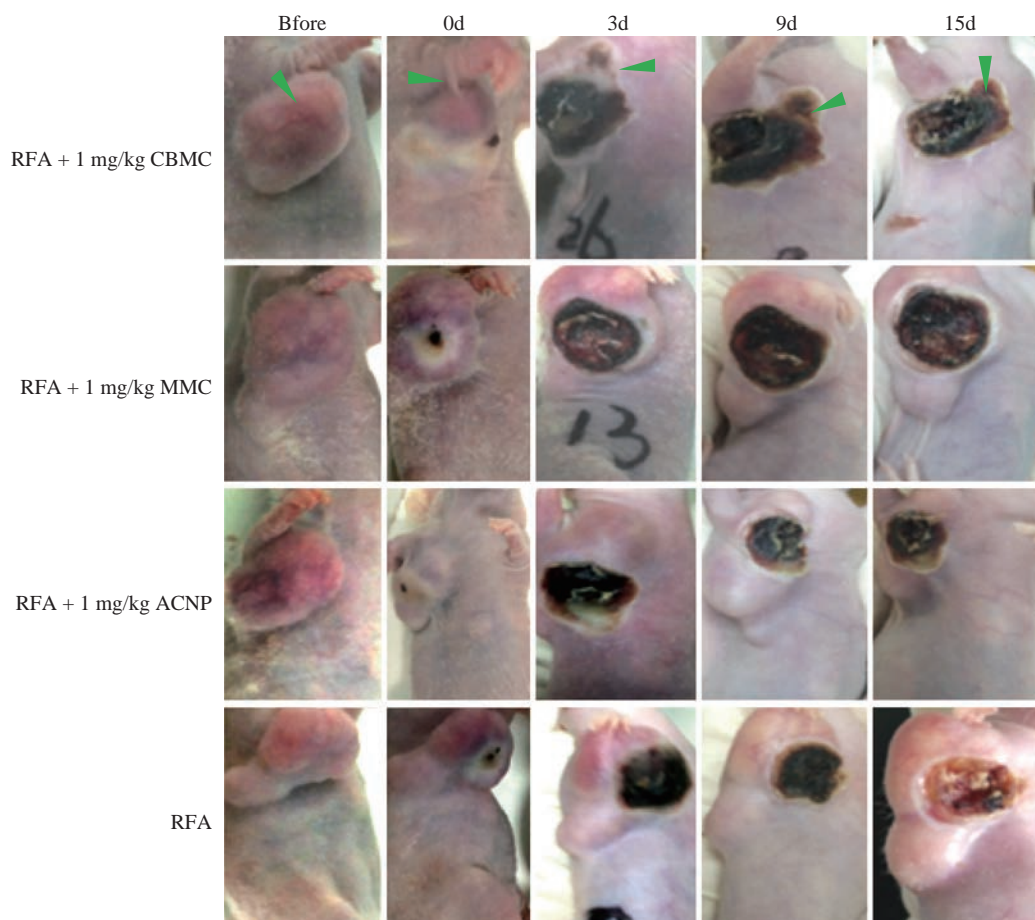


Fig. 3 Tumor growth state of nude mice at different times after treatment.

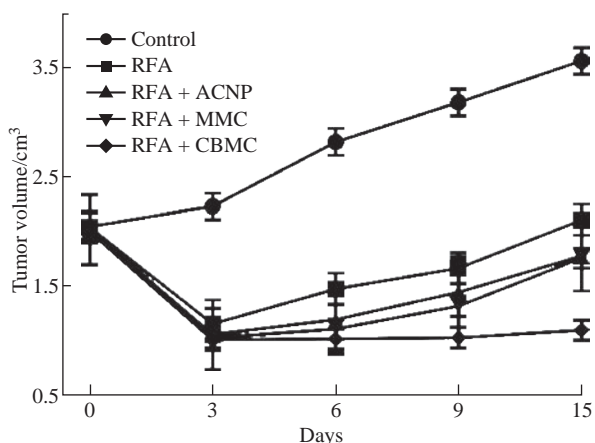


Fig. 4 The tumor growth curve of nude mice in the different groups.

stronger inhibitor of tumor relapse than MMC. The tumor growth curves (Fig. 4) confirmed that CBMC was more effective than MMC. Between days zero and three posttreatment, the tumor growth curves of RFA+MMC and RFA+CBMC were similar. From day six onwards, their tumor growth curve became more distinct as the tumor size of the RFA+MMC group

started to increase at a similar rate as observed in the RFA only and RFA+ACNP groups while tumor growth was almost negligible for the RFA+CBMC group. By day 15, no newborn tumors appeared around the RFA focus in two out of six model mice treated with RFA+CBMC. Amazingly, one of the RFA+CBMC treated model mice had a small tumor at the edge of the scab which continued to decrease in size, and nearly disappeared by day 15 (Fig. 4, arrows). This recovery was accompanied by the growth of normal surrounding tissues towards the center of the RFA focuses. Despite its rarity, this phenomenon should not be neglected. Taken together, the above results indicated that only the concomitant treatment of RFA and CBMC had a significant inhibitory effect on post-RFA recurrent tumors.

Histopathological observations after RFA

Fig. 5 shows the results of our histopathological observations. In the HE-stained sections of the RFA only and the RFA+ACNP group, there was a large number of necrotic cell fragments at the center of the RFA focuses and residual tumor cells could be seen

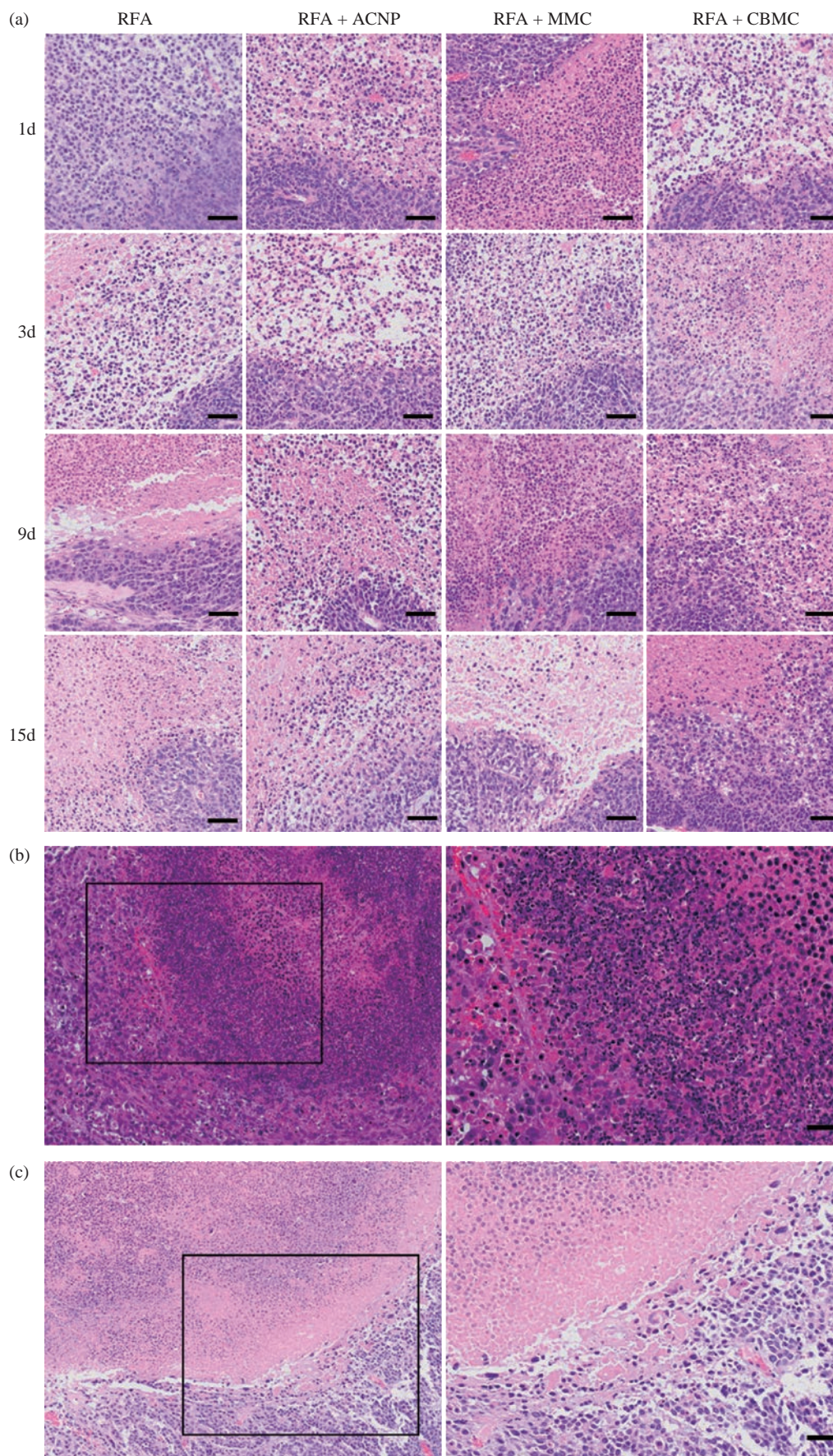


Fig. 5 Pathological change of the tumor in different groups of nude mice by HE staining. **(a)** Pathological change of the tumors in different groups at different times. Pathological change of the tumors in the RFA+CBMC group **(b)** nine days and **(c)** 15 days after the treatment. Scale bar = 10 μ m.

in the surrounding transition tissues on day one after RFA. Three days after the treatment, the cell fragments in the RFA center had decreased and more proliferative tumor cells were seen in the transition tissues. By day nine, the tumor cells had actively proliferated and began to migrate toward the RFA focuses. Finally, 15 days posttreatment, large tumor cells migrated to the RFA focuses, the transition area disappeared, and cancer nests were formed at the edge of RFA focuses (Fig. 5, arrows) and were accompanied by the macroscopic fusion of tumors. In the HE-stained histopathological sections of RFA+MMC treated mice, there were less residual tumor cells in the surrounding tissues compared to the RFA only group on the first day post-RFA. With time, the proliferation of residual tumor cells was as profound as in the RFA only group and cancer nests were formed (Fig. 5, arrows). On day 15, there were no significant histopathological differences between the RFA+MMC group and the RFA only group. In the HE-stained histopathological sections of RFA+CBMC treated mice, the number of residual tumor cells was the same as in RFA+MMC mice on day zero. However, with time, the number of

proliferative tumor cells decreased in RFA+CBMC treated mice in comparison to any other treatment group, and also no cancer nests were formed (Fig. 5). These results explain histopathologically why RFA+CBMC treated mice had the smallest number of recurrent tumors out of all experimental groups.

Immunohistochemical staining with apoptotic and cell proliferation markers after RFA

Fig. 6 shows immunohistochemical staining of tissues with apoptotic and cell proliferation markers following RFA. Caspase-3 is a commonly used apoptosis marker; red immunofluorescence of the tissue meant that it was rhodamine anti-caspase-3 positive, thereby identifying the apoptotic cells. There were a large number of apoptotic cells on day one following RFA. Their numbers significantly decreased by day three and almost disappeared in the RFA only and RFA+ACNP treated mice. In the RFA+CBMC treated mice, there were more apoptotic tumor cells at any given time. In the RFA+MMC group, there were more apoptotic cells than in the RFA only group one day after the treatment. These differences were

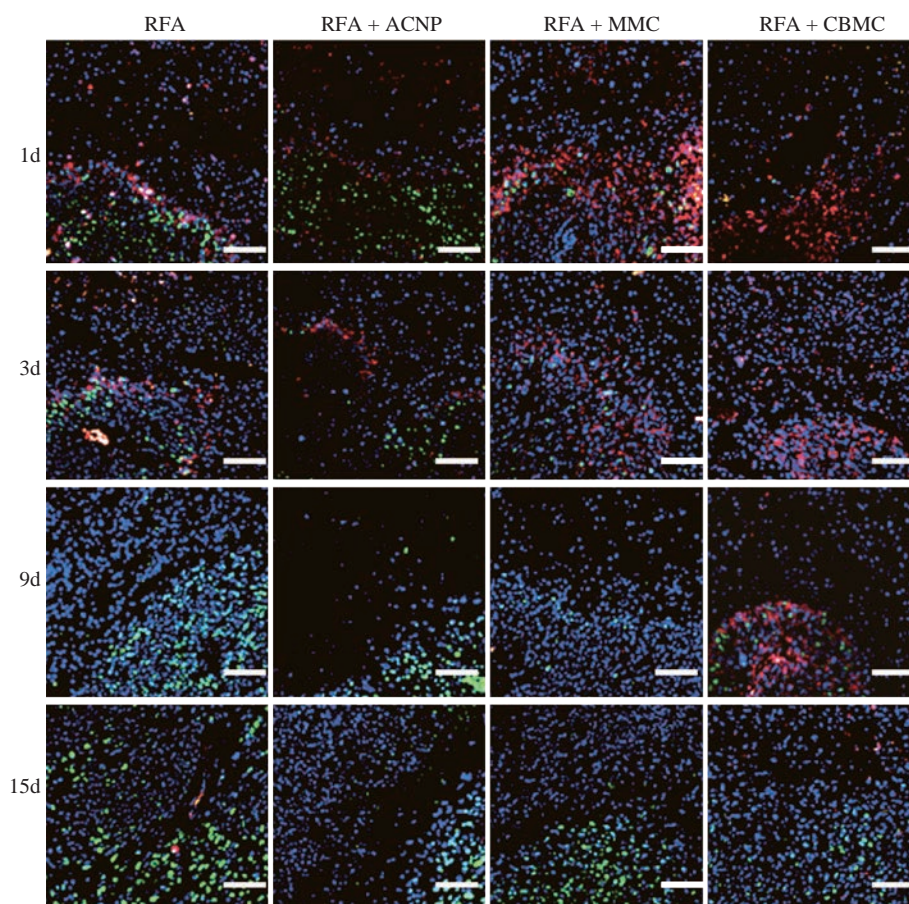


Fig. 6 Immunohistochemical staining of tumor cell proliferation and apoptosis. Red immunofluorescence marked rhodamine anti-caspase-3, green staining marked FITC anti-PCNA, and the blue fluorescence is DAPI stained nuclei. Scale bar = 10 μ m.

no longer observed on the subsequent days. PCNA is a marker for cell proliferation and positive staining identifies actively proliferating cells. Immunological staining revealed that the number of proliferating cells gradually increased and that, with time, they migrated towards the inside of the RFA focus (Fig. 6). The most active proliferating tumor cells were observed in the RFA only and RFA+ACNP groups, while tumor cells in the RFA+CBMC mice were least proliferating. The extent of tumor cell proliferation in the RFA+MMC group was between that observed in the RFA+CBMC group and the RFA only group. The immunohistochemical staining presented in this study, therefore, indicated that both MMC and CBMC act synergistically with the RFA treatment. However, the effect of MMC was only temporary whereas CBMC was able to inhibit the post-RFA recurrence of tumors. The results furthermore suggested that the stimulation of apoptosis and the concomitant suppression of tumor cell proliferation are key to preventing post-RFA tumor relapse when co-administered with CBMC.

Conclusions

The RFA technology has recently been successfully used for the treatment of liver cancer, lung cancer, pancreatic cancer, as well as other solid tumors in adrenal glands, kidneys, and breasts [6]. However, RFA also has some limitations as a tumor therapy [37]. Due to its irregular and invasive features, the tumor growth will lead to incomplete tumor ablation and, because any residual tumor tissue can rapidly grow when in a nutrient-rich environment (blood supply), tumor relapses are often experienced. Some researchers have even suggested that RFA treatment could stimulate the rapid growth of incomplete ablated tumor cells. Our *in vitro* study showed that RFA does not stimulate cell growth around the ablation focus [38]. The data, therefore, confirmed that incomplete ablation is the principal cause of post-RFA tumor recurrence.

To improve the RFA treatment and prevent residual tumors from growing, this study used the mesoporous ACNP to adsorb MMC and developed a nano drug delivery system (NDDS) where ACNP acts as the carrier of the MMC drug. ACNP was chosen because of its; longevity in target tissues [36]; large drug loading capacity, due to their graphene composition [39] and the tortuous nanopores deepening into the core of the particles; wide adsorption spectrum and great inner absorption area [37]; and nontoxicity [40]. MMC is a

proven effective anticancer drug [35] capable of almost completely killing the human stomach cancer BGC-823 cells. Its clinical use is however limited due to its short *in vivo* half-life [41] and toxicity [41], making MMC a highly effective candidate to use concomitantly with RFA.

The experimental results suggest that focally injected CBMC could increase the RFA scope and inhibit the post-RFA tumor growth more effectively than when MMC is injected directly. Although the detailed mechanism remains unclear, the positive effects of CBMC are attributed to its slow release of MMC cargoes over a long period of time. Consequently, an effective MMC concentration can be maintained and suppress the growth of residual tumor cells in the RFA focus. A well-known mechanism for injected nano drug delivery systems (NDDS) to increase the drug concentration in tumors is the enhanced permeability and retention (EPR) effect [26]. The basic principle of the EPR effect is that NDDS can enter the tumor tissues through the vascular capillary endothelial pores and gaps and that, once entered, they become less prone to reversely diffusing back to the blood circulation. NDDS are thus retained in the tumor tissues where they can slowly release their drug cargoes [26]. In the study presented herein, we took advantage of the ACNP characteristics, one of them being that ACNP is larger (250 nm) than the vascular endothelial pores and gaps, and used it to carry MMC. After RFA, the blood vessels and lymphatic vessels at the edge of the focus become coagulated. As a result, the focally injected CBMC was able to release its cargo without MMC immediately dissipating into the bloodstream. This slow and steady release of MMC then continually inhibited post-RFA tumor recurrence. As already highlighted, MMC is a small molecule drug and is easily absorbed into the blood circulation. Therefore, when not applied as an NDDS, MMC cannot maintain its concentration in the RFA focuses for as long as CBMC. For this reason, the capillary endothelial pore and gap size was used as a guide for this study to choose the NDDS to be used in conjunction with RFA, which is in agreement with the literature [31, 32, 34].

The key for NDDS to inhibiting tumor recurrence after RFA was the slow release of the drugs into the tumor tissue and maintenance of the drug concentration at an effective level over a long period of time. This study demonstrated that CBMC has a very small drug release rate constant and a very long half-life

in tumor tissue liquid. CBMC, therefore, has all the requirements to inhibit tumor recurrence effectively after RFA treatment. Compared with CBMC, free MMC also has a certain therapeutic effect on tumor recurrence after RFA treatment. Particularly at the early stages following treatment, the response to free MMC was similar to CBMC in terms of curbing recurrence and growth of the tumor. However, the tumor size-time (S-t) curve of free MMC steepened and separated from the S-t curve for CBMC between days nine to 15 posttreatment. These observations confirmed that the effectiveness of CBMC on post-RFA tumor recurrence is linked to the slow release and the long-term maintenance of an effective concentration of the therapeutic agent.

To conclude, our research provided proof that the tumor recurrence after RFA is due to hyperplasia of residual tumor cells. We also demonstrate that focal injection of anti-tumor drugs, particularly as NDDS, can shape the future of RFA.

Acknowledgments

This work was supported by the National Key Basic Research Program (973 Project) (No. 2010CB933904), the Foundation of General Logistics Department of PLA (DWS16J007) and a Military Medical Scientific and Technological Project for the "Twelfth Five-year Plan" (AWS15J007).

Conflict of Interests

The authors declare that no competing interest exists.

References

- [1] American Cancer Society. Cancer Facts and Figures 2013. American Cancer Society, 2013.
- [2] S. Rossi, F. Fornari, and L. Buscarini, Percutaneous ultrasound-guided radiofrequency electrocautery for the treatment of small hepatocellular carcinoma. *Journal of Interventional Radiology*, 1993, 8(3): 97-103.
- [3] C.H. Yuan, D.R. Xiu, H.Y. Ge, et al., Ultrasound guided ablation therapy of hepatic colorectal metastases: initial experience of real time virtual sonography navigation system. *Beijing Da Xue Xue Bao*, 2013, 45(6): 956-959.
- [4] A.H. Lay, J. Stewart, N.E. Canvasser, et al., Likelihood of incomplete kidney tumor ablation with radio frequency energy: Degree of enhancement matters. *J Urol*, 2016, 196(1): 41-45.
- [5] D. Chudasama, A. Rice, V. Anikin, et al., Circulating tumour cells in patients with malignant lung tumors undergoing radio-frequency ablation. *Anticancer Res*, 2015, 35(5): 2823-2826.
- [6] T. Nakazawa, S. Kokubu, A. Shibuya, et al., Radiofrequency ablation of hepatocellular carcinoma: correlation between local tumor progression after ablation and ablative margin. *AJR Am J Roentgenol*, 2007, 188(2): 480-488.
- [7] Y. Inoue, J. Hiro, Y. Toiyama, et al., Optimal use of current chemotherapy in multimodality therapy for advanced colorectal cancer. *Oncol Lett*, 2012, 3(2): 363-368.
- [8] I. Smith, M. Kahaleh, Biliary Tumor ablation with photodynamic therapy and radiofrequency ablation. *Gastrointest Endosc Clin N Am*, 2015, 25(4): 793-804.
- [9] M. Nikfarjam, V. Muralidharan, and C. Christophi, Mechanisms of focal heat destruction of liver tumors. *J Surg Res*, 2005, 127(2): 208-223.
- [10] S. McDermott, D.A. Gervais, Radiofrequency Ablation of liver tumors. *Seminars in Interventional Radiology*, 2013, 30(1): 49-55.
- [11] Z. Lu, M. Tsai, D. Lu, et al., Tumor-penetrating microparticles for intraperitoneal therapy of ovarian cancer. *J Pharmacol Exp Ther*, 2008, 327(3): 673-682.
- [12] G.R. Dakwar, E. Zagato, J. Delanghe, et al., Colloidal stability of nano-sized particles in the peritoneal fluid: towards optimizing drug delivery systems for intraperitoneal therapy. *Acta Biomater*, 2014, 10(7): 2965-2975.
- [13] O.M. Sarhan, R.M. Hussein, Effects of intraperitoneally injected silver nanoparticles on histological structures and blood parameters in the albino rat. *Int J Nanomedicine*, 2014, 9: 1505-1517.
- [14] D. Cui, L. Ma, X. Zhi, et al., Advances and prospects of nanotheranostic technology for gastric cancer. *Nano Biomedicine and Engineering*, 2016, 8(4): 219-239.
- [15] H. Fu, New developments of gastric cancer biomarker research. *Nano Biomedicine and Engineering*, 2016, 8(4): 268-273.
- [16] K. Inoue, H. Onishi, Y. Kato, et al., Comparison of intraperitoneal continuous infusion of floxuridine and bolus administration in a peritoneal gastric cancer xenograft model. *Cancer Chemother Pharmacol*, 2004, 53(5): 415-422.
- [17] O. Stoeltzing, W. Liu, N. Reinmuth, et al., Inhibition of integrin alpha5beta1 function with a small peptide (ATN-161) plus continuous 5-FU infusion reduces colorectal liver metastases and improves survival in mice. *Int J Cancer*, 2003, 104(4): 496-503.
- [18] J. Fujiyama, Y. Nakase, K. Osaki, et al., Cisplatin incorporated in microspheres: development and fundamental studies for its clinical application. *J Control Release*, 2003, 89(3): 397-408.
- [19] L. De Smet, W. Ceelen, J.P. Remon, et al., Optimization of drug delivery systems for intraperitoneal therapy to extend the residence time of the chemotherapeutic agent. *Scientific World Journal*, 2013, 2013: 720858.
- [20] Z.L. Feng, L.B. Chen, Z.Y. Liu, et al., DCF intraperitoneal and intravenous dual chemotherapy regimen for advanced gastric cancer: A feasibility study. *Oncol Lett*, 2015, 9(1): 491-497.
- [21] N. Gould, M.W. Sill, R.S. Mannel, et al., A phase I study with an expanded cohort to assess feasibility of intravenous docetaxel, intraperitoneal carboplatin and intraperitoneal paclitaxel in patients with previously untreated ovarian, fallopian tube or primary peritoneal carcinoma: A gynecologic oncology group study. *Gynecol Oncol*, 2012, 127(3): 506-510.
- [22] J. Xie, Y. Yong, X. Dong, et al., Therapeutic nanoparticles based on curcumin and bamboo charcoal nanoparticles for chemo-photothermal synergistic treatment of cancer and radioprotection of normal cells. *ACS Appl Mater Interfaces*, 2017, 9(16): 14281-14291.

- [23] S.K. Lai, D.E. O'Hanlon, S. Harrold, et al., Rapid transport of large polymeric nanoparticles in fresh undiluted human mucus. *Proc Natl Acad Sci USA*, 2007, 104(5): 1482-1487.
- [24] A.W. Carpenter, D.L. Slomberg, K.S. Rao, et al., Influence of scaffold size on bactericidal activity of nitric oxide-releasing silica nanoparticles. *ACS Nano*, 2011, 5(9): 7235-7244.
- [25] F. Gentile, A. Curcio, C. Indolfi, et al., The margination propensity of spherical particles for vascular targeting in the microcirculation. *J Nanobiotechnology*, 2008, 6: 9.
- [26] E.A. Nance, G.F. Woodworth, K.A. Sailor, et al., A dense poly(ethylene glycol) coating improves penetration of large polymeric nanoparticles within brain tissue. *Sci Transl Med*, 2012, 4(149): 149ra119.
- [27] H. Iwasa, H. Kondo, Differences in the width of the intercellular spaces in the epithelial basal infolding and the renal glomerular filtration site between freeze-substitution and conventional fixation. *J Anat*, 1999, 194(Pt 2): 215-221.
- [28] H. Sarin, Physiologic upper limits of pore size of different blood capillary types and another perspective on the dual pore theory of microvascular permeability. *J Angiogenesis Res*, 2010, 2: 14.
- [29] D. Lembo, R. Cavalli, Nanoparticulate delivery systems for antiviral drugs. *Antivir Chem Chemother*, 2010, 21(2): 53-70.
- [30] I.I. Slowing, J.L. Vivero-Escoto, C.W. Wu, et al., Mesoporous silica nanoparticles as controlled release drug delivery and gene transfection carriers. *Adv Drug Deliv Rev*, 2008, 60(11): 1278-1288.
- [31] Y.T. Liao, C.H. Liu, J. Yu, et al., Liver cancer cells: targeting and prolonged-release drug carriers consisting of mesoporous silica nanoparticles and alginate microspheres. *Int J Nanomedicine I*, 2014, 9: 2767-2778.
- [32] J.L. Vivero-Escoto, I.I. Slowing, B.G. Trewyn, et al., Mesoporous silica nanoparticles for intracellular controlled drug delivery. *Small*, 2010, 6(18): 1952-1967.
- [33] D.K. Armstrong, G.F. Fleming, M. Markman, et al., A phase I trial of intraperitoneal sustained-release paclitaxel microspheres (Paclimer) in recurrent ovarian cancer: A gynecologic oncology group study. *Gynecol Oncol*, 2006, 103(2): 391-396.
- [34] Y.L. Colson, R. Liu, E.B. Southard, et al., The performance of expansile nanoparticles in a murine model of peritoneal carcinomatosis. *Biomaterials*, 2011, 32(3): 832-840.
- [35] Q. Qiulian, Z. Yingge, Y. Liuzhong, et al., Intraperitoneal chemotherapy with mitomycin C bound to activated carbon nanoparticles for nude mice bearing human gastric carcinoma. *Chin J Oncol*, 2006, 28(4): 257-260.
- [36] Y. Liuzhong, Z. Yingge, Pharmacokinetic study of intraperitoneal chemotherapy with mitomycin C absorbed to activated carbon particles in rats. *Chin J Cancer Prev Treat*, 2008, 15(20): 1548-1551.
- [37] T. Shimizu, S. Murata, H. Sonoda, et al., Hyperthermic intraperitoneal chemotherapy with mitomycin C and 5-fluorouracil in patients at high risk of peritoneal metastasis from colorectal cancer: A preliminary clinical study. *Mol Clin Oncol*, 2014, 2(3): 399-404.
- [38] B. Zhao, L. Sun, W. Zhang, et al., Secretion of intestinal goblet cells: a novel excretion pathway of nanoparticles. *Nanomedicine*, 2014, 10(4): 839-849.
- [39] M. Kudo, Local ablation therapy for hepatocellular carcinoma: current status and future perspectives. *J Gastroenterol*, 2004, 39(3): 205-214.
- [40] Y.T. Li, C. Nie, W.T. Pan, et al., Effects of radiofrequency ablation on growing status of tumor cells around the focus of ablation. *Journal of International Pharmaceutical Research*, 2013, 40(5): 599-604.
- [41] Z. Liu, J.T. Robinson, X. Sun, et al., PEGylated nanographene oxide for delivery of water-insoluble cancer drugs. *J Am Chem Soc*, 2008, 130(33):10876-10877.
- [42] Z. Yang, S.Z. Ma, and Y.G. Zhang, Using activated carbon nanoparticles to decrease the genotoxicity and teratogenicity of anticancer therapeutic agents. *J Nanosci Nanotechnol*, 2010, 10(12): 8603-8609.
- [43] R. Yeung, Y. McConnell, G. Roxin, et al., One compared with two cycles of mitomycin C in chemoradiotherapy for anal cancer: Analysis of outcomes and toxicity. *Curr Oncol*, 2014, 21(3): e449-e456.

Copyright© Yueting Li, Baoquan Zhao, Yunzhu Pu, Weitong Pan, Xiaoman Li, Yuxia Wang, Yongan Wang, Lan Sun, Chunqian Huang, Qian Li, and Yingge Zhang. This is an open-access article distributed under the terms of the Creative Commons Attribution License, which permits unrestricted use, distribution, and reproduction in any medium, provided the original author and source are credited.